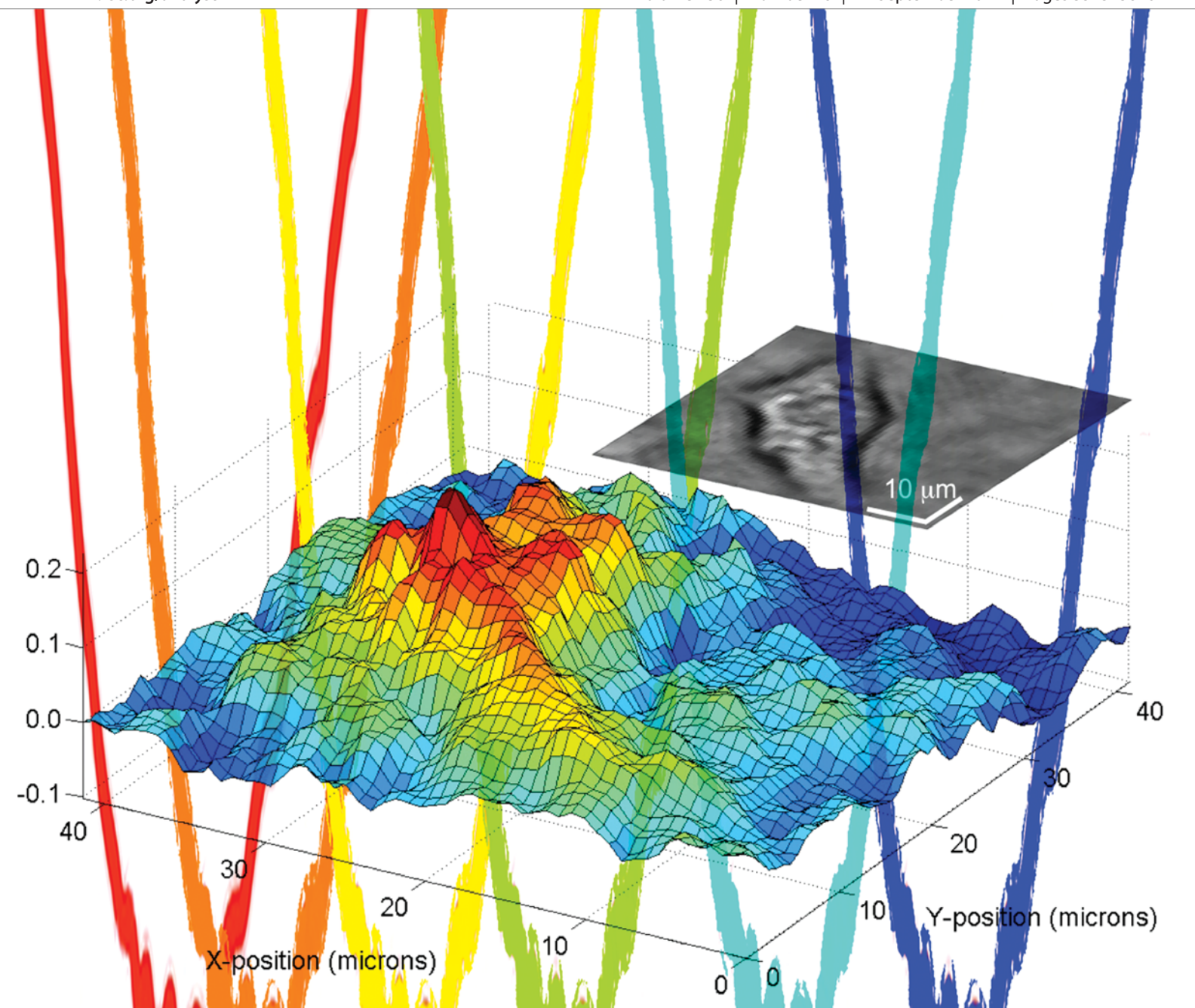


Analyst

Interdisciplinary detection science

www.rsc.org/analyst

Volume 136 | Number 18 | 21 September 2011 | Pages 3573–3816



ISSN 0003-2654

RSC Publishing

PAPER

Erich A. Lidstone *et al.*
Label-free imaging of cell attachment with
photonic crystal enhanced microscopy

Cite this: *Analyst*, 2011, **136**, 3608

www.rsc.org/analyst

PAPER

Label-free imaging of cell attachment with photonic crystal enhanced microscopy†‡§

Erich A. Lidstone,^{¶*a} Vikram Chaudhery,^{¶*b} Anja Kohl,^{¶*ac} Vincent Chan,^a Tor Wolf-Jensen,^e Lawrence B. Schook,^{de} Rashid Bashir^{ab} and Brian T. Cunningham^{ab}

Received 27th February 2011, Accepted 22nd May 2011

DOI: 10.1039/c1an15171a

We introduce photonic crystal enhanced microscopy (PCEM) as a label-free biosensor imaging technique capable of measuring cell surface attachment and attachment modulation. The approach uses a photonic crystal optical resonator surface incorporated into conventional microplate wells and a microscope-based detection instrument that measures shifts in the resonant coupling conditions caused by localized changes in dielectric permittivity at the cell-sensor interface. Four model systems are demonstrated for studying cancer cells, primary cardiac muscle cells, and stem cells. First, HepG2/C3 hepatic carcinoma cells were cultured and observed *via* PCEM in order to characterize cell adhesion in the context of growth and locomotion. Second, Panc-1 pancreatic cancer cells were used to verify that cell attachment density decreases in response to staurosporine, a drug that induces apoptosis. Third, we used PCEM to confirm the influence of integrin-mediated signaling on primary neonatal cardiomyocyte growth and development. Rounded cardiomyocytes consistently showed decreased cell attachment density as recorded *via* PCEM, while spreading cells exhibited greater attachment strength as well as increased contractility. Finally, PCEM was used to monitor the morphological changes and extracellular matrix remodeling of porcine adipose-derived stem cells subjected to a forced differentiation protocol. Each of these experiments yielded information regarding cell attachment density without the use of potentially cytotoxic labels, enabling study of the same cells for up to several days.

Introduction

Cell adhesion is a vital process for cell growth, proliferation, differentiation and motility, playing a central role in such varied phenomena as tissue growth and development, inflammation, wound healing, cancer metastasis, and myriad others.^{1,2} For life science research and cell-based pharmaceutical screening

applications, development of a more fundamental understanding of the factors influencing cell-substrate interactions requires the development of new tools. Current *in vitro* cell imaging techniques often rely either on cytotoxic stains or fluorescent labels to provide highly specific information; both of these techniques frequently permanently alter the state of the cell, and often require fixing or isolation of the samples to be considered for examination. Traditional light microscopy and phase contrast microscopy offer improvements in the lengths of possible experimentation, but at the expense of specific and relevant information regarding cell activity and metabolism. Here, we present photonic crystal enhanced microscopy (PCEM) as a label-free imaging biosensor technique for visualizing and quantifying complex cellular responses to multiple stimuli over prolonged periods of study.

Photonic Crystal (PC) biosensors have been recently demonstrated as a high-resolution label-free detection technology that can be fabricated from plastic materials and incorporated into standard microplate formats for high throughput screening applications.^{3,4} PC biosensors consist of a low refractive index sub-wavelength periodic grating structure that functions as a highly reflective optical resonator (see Supplementary Fig. 1 online†). While previously reported PC surfaces (also referred to

^aDepartment of Bioengineering, UIUC, Urbana, IL

^bDepartment of Electrical and Computer Engineering, UIUC, Urbana, IL

^cUS Army Corps of Engineers Construction Engineering Research Laboratory, Champaign, IL

^dDepartment of Veterinary Pathobiology, UIUC, Urbana, IL

^eDepartment of Animal Sciences, UIUC, Urbana, IL

† Electronic supplementary information (ESI) available. See DOI: 10.1039/c1an15171a

‡ Author Contributions: E. A. L., V. C., and A. K. designed each of the experiments, fabricated the PC biosensors, and conducted the experiments described in this manuscript. V. C. and R. B. enabled and contributed to work with cardiomyocytes and porcine adipose-derived stem cells. T. W. J. and L. B. S. contributed to work involving porcine adipose-derived stem cells. B. T. C. was engaged as the principal investigator throughout this work.

§ Competing Interests Statement: B. T. C. is the Chief Technology Officer of SRU Biosystems, Woburn, MA, US.

¶ These authors contributed equally to the completion of this work.

as Guided Mode Resonant Filters) have been comprised of a rectangular grating profile with a period of 550 nm and a grating depth of approximately 150 nm, the biosensors used in this study have been modified to reduce possible effects of sensor morphology on the formation of cell attachments. To reduce the occurrence of such effects, the PC biosensors used in this study possess a period of 360 nm with a grating depth of approximately 30 nm. The addition of an intermediary SiO₂ layer allows for the exposed TiO₂ layer of the sensor to be deposited with a gradual curved profile in lieu of the rectangular profile used in previously documented sensors. Atomic force microscopy imaging was performed to verify surface morphology would have a minimal effect on cellular activity (see Supplementary Figure 1, online†). It is worth noting that none of the cells investigated in this work exhibited polarization with respect to the grating structure. When illuminated by a collimated laser, the PC surface acts as a highly efficient light reflector only at a specific angle of incidence at which resonant coupling of incident light to the PC occurs (see Supplementary Fig. 1 online†). The resonant coupling angle is dependent upon the dielectric permittivity of material on the PC surface, and shifts to lower angles when cells or biomolecules become attached. Because the PC surface effectively prevents lateral propagation of resonantly coupled light, attachment of discrete objects, such as cells, results in a highly localized shift in the resonant coupling angle, thus opening up the potential for high resolution biosensor imaging. In this report, we present the use of a detection system based upon microscopy that overcomes spatial resolution limitations of previously reported PC biosensor imaging systems^{5,6} enabling, for the first time, label-free cell attachment images with 0.61 μm² pixel resolution. The detection system does not require physical contact to a coupling prism as required for imaging Surface Plasmon Resonance (SPR),^{7,8} nor the *a priori* knowledge of the analyte necessary for ellipsometry,^{9,10} therefore enabling high throughput measurement of large numbers of cells within biosensor-embedded microplates, flow channels, and culture dishes.

As shown in Supplementary Fig. 2 online,† the PCEM instrument illuminates the PC surface from below with a collimated laser beam, which is rapidly scanned through a ~3° range of incident angles at 0.01-degree increments with a computer-controlled rotating mirror. An image of transmitted light intensity is gathered through a 10x or 20x microscope objective onto a CCD camera for each incident angle (see Supplementary Fig. 1 online†). At the resonant coupling angle, the incident laser light is efficiently reflected, resulting in a minimum in transmitted intensity. Software determines the Angle of Minimum Transmission (AMT) on a pixel-by-pixel basis from the CCD images by fitting a second order polynomial function to the transmitted intensity *versus* angle curve (Fig. 1c). It is important to note that due to the limited penetration of the evanescent field region from the PC into the surrounding cell media (approx. 100 nm), PCEM is sensitive only to dynamic changes in biomaterial density at or near the cell surface, remaining unaffected by the presence and location of cellular organelles. As attachment, driven by the activity of integrins and filopodia, draws the cell into more intimate contact with the PC surface, there is a commensurate increase in the local dielectric permittivity that is clearly measurable (Fig. 1, Supplementary Fig. 4†).³ Detection

resolution is sufficient not only for observation of large angle shifts that differentiate cell from non-cell regions, but also for observation of subtle changes in attachment strength that result from motility, apoptosis, differentiation, and contraction.

Materials and methods

Instrument description

The detection system used in our study is a modified back-illuminated fluorescent microscope (Olympus BX51WI) shown schematically in Supplementary Figure 2. The microscope is equipped with 10x and 20x objective lenses (N.A. = 0.25, 0.40, respectively) and an electron multiplying CCD (C9100-13 EM-CCD; Hammamatsu Inc.) for imaging. A 300-mW, λ = 637 nm AlGaInP diode laser is the excitation source. The laser light is passed through a rotating diffuser and then collimated by a beam expander. This sequence of optical components results in a spatially uniform, highly collimated beam that is then incident on a high-resolution motorized gimbal-mounted mirror, thus providing collimated illumination at a user-selectable incident angle. In order to maintain a constant illumination area on the device, the gimbal-mounted mirror sits on top of a motorized linear stage that translates laterally as the mirror rotates. As the collimated light at a fixed wavelength is incident on the PC surface, the angle of incidence can be tuned to allow the laser to couple with the PC resonance, thereby allowing maximum field coupling into the transverse electric (TE) mode of the PC. The excitation illumination was TE polarized by passing the laser light through a half-wave plate.

Device fabrication

Fabrication of the device was performed using a plastic-based nanoreplica molding process.³ Briefly, a silicon wafer with a negative surface volume image of the desired grating pattern was fabricated using deep-UV lithography and reactive ion etching. A liquid that contains an uncured monomer and a UV-activated polymerization initiator is sandwiched between a flexible plastic sheet and the silicon master wafer to enable the liquid to fill the silicon surface structure subsequent to curing with a high intensity UV lamp (Xenon, Inc). The hardened polymer grating preferentially adheres to the plastic substrate, and thus can be easily peeled away from the silicon. After the molding step, the replica was cut and attached to a 1 × 3 in² microscope slide. An evaporated SiO₂ intermediate layer, (t_{SiO₂}) = 200 nm, (e-beam evaporation, Denton Inc.) was deposited on the grating surface to control the resonant peak width. After the SiO₂ deposition, ~60 nm of TiO₂ was deposited by RF sputtering (PVD 75, Kurt Lesker) using an *in situ* process monitor to accurately achieve a resonance condition that nominally results in λ = 637 nm wavelength resonantly coupling to the PC surface at an incident angle of 4° in an aqueous environment. The device is bonded to a six well bottomless microplate using a transparent UV-curable adhesive (AC R260-A1, Addison Clear Wave). The plates were thoroughly rinsed and the wells were incubated with 70% ethanol for 15 min.

For Panc-1 and HepG2/C3 cell culture, the PC biosensors were coated with poly-*D*-lysine (MW = 70,000–150,000 Da, Sigma-Aldrich P6407) immediately prior to plating cells. For this

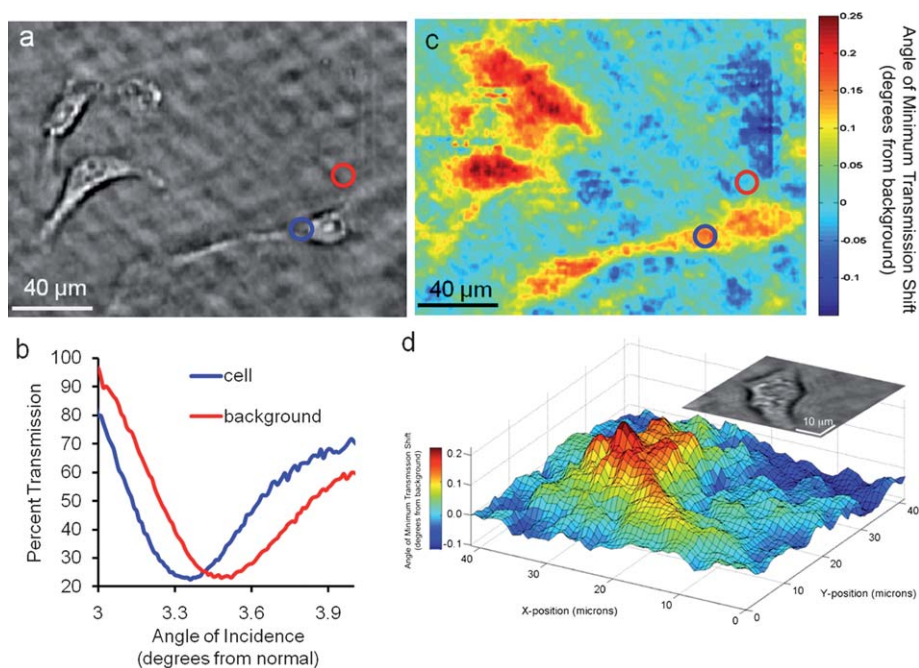


Fig. 1 Summary of Photonic Crystal Enhanced Microscopy. a) Bright field microscopy of HepG2/C3 cells shows cell spreading and morphology. b) Transmission intensity is plotted as a function of angle of incidence for individual pixels on (blue) and off (red) a cell. Pixel regions are highlighted in (a). c) A composite PCEM image, describes the angle of minimum transmission (AMT) as a function of position. Attachment proteins deposited on the biosensor by viable cells result in a reduced angle of minimum transmission shift. d) A surface plot of cardiomyocyte attachment at 24h obtained *via* PCEM corresponds with the morphology observed in bright field microscopy (inset).

purpose the wells were incubated with a 100 ng ml^{-1} solution in cell grade phosphate buffered saline (PBS), $\text{pH} = 7.4$ for 15 min. After incubation, the wells were rinsed twice with PBS before cell media was added. For cardiomyocyte culture, bare sensor wells remained uncoated while fibronectin- and collagen-coated wells were rinsed with PBS before the addition of 2.0 ml of a solution containing $5.0 \text{ } \mu\text{g ml}^{-1}$ fibronectin (Sigma-Aldrich F0895) and $20.0 \text{ } \mu\text{g ml}^{-1}$ collagen (Sigma-Aldrich C8919) diluted in PBS. Wells were then incubated for 1 h at $37 \text{ }^\circ\text{C}$ before rinsing three times with PBS. For adipose-derived stem cell culture, wells were rinsed with PBS prior to 1 h incubation with 2.0 mL $25 \text{ } \mu\text{g mL}^{-1}$ collagen (Sigma Aldrich C8919) dissolved in 0.1M acetic acid in ultrapure water at $37 \text{ }^\circ\text{C}$. Wells were then rinsed three times with PBS immediately prior to cell culture.

Materials and cell culture

Cell culture media was obtained from the Cell Media Facility at the University of Illinois at Urbana-Champaign. Panc-1 cells, porcine adipose-derived stem cells, and neonatal rat cardiomyocytes were cultured in Dulbecco's modified Eagle's medium (DMEM) with 10% fetal bovine serum (FBS), 4 mM L-glutamine and penicillin-streptomycin. The HepG2/C3 cells were grown in minimum essential medium (MEM) with 10% FBS. PBS ($\text{pH} 7.4$) and poly-d-lysine (mol wt 70–150,000) were purchased from Sigma-Aldrich and trypsin (0.25% + EDTA) from Thermo scientific. Staurosporine was purchased from Sigma-Aldrich and dissolved in DMSO leading at a concentration of 1 mg/ml .

All cell lines were grown in an incubator at $37 \text{ }^\circ\text{C}$ and 5% CO_2 until 80% confluence and then passed using trypsin every 2–5

days as necessary. For imaging the cells were centrifuged to remove the trypsin and then resuspended in media and plated on the device in a total volume of 2 ml at a density of $4\text{--}6 \times 10^4$ cells/mL. Cell counting was performed with a hemacytometer (Reichert).

Cardiomyocyte isolation and culture

Cardiomyocytes were obtained from 6-day old neonatal Sprague-Dawley rats (Harlan Laboratories, Inc.) using an approved protocol by the University of Illinois at Urbana-Champaign Institutional Animal Care and Use Committee (IACUC; Protocol #08190, Adopted from Maass *et al.*,¹²). Briefly, whole hearts were excised from the rats and placed in $4 \text{ }^\circ\text{C}$ HBSS buffer. Using small scissors, the left and right atria were removed and the remaining ventricles were quartered. The quartered ventricles were digested in 0.05% (w/v) purified trypsin (Worthington Biochemicals Corp.), while rotating gently at $4 \text{ }^\circ\text{C}$ overnight. After 16 h, warm growth medium was added for 5 min at $37 \text{ }^\circ\text{C}$ to inhibit trypsin digestion. After washing and discarding the supernatant, 0.1% (w/v) purified type II collagenase (Worthington Biochemicals Corp.) was added for 45 min while rotating at $37 \text{ }^\circ\text{C}$. The tissue was gently triturated to mechanically loosen the cells, and the suspension was filtered through a $40\text{-}\mu\text{m}$ cell strainer. The suspension was removed after centrifugation at $150 \times g$ for 6 min. The remaining cell pellet was re-suspended in warm growth medium and pre-plated for 1 h to enrich for cardiomyocytes. The suspension was collected, and cardiomyocytes were seeded on polystyrene dishes. The growth medium consisted of high glucose (4.5 g L^{-1}) DMEM with 10% FBS. The cells were cultured in an incubator with 5% CO_2 at $37 \text{ }^\circ\text{C}$.

Porcine adipose-derived stem cell isolation

Adipose-derived stem cells were isolated from back fat of pigs that were 3 months of age, in compliance with University of Illinois IACUC approved procedures. Pigs were euthanized by an overdose of pentobarbital and fat samples were excised from the back proximal to the spine. Adipose tissues were cleaned and submerged in PBS (without Ca or Mg) containing 3X Penicillin/Streptomycin prior to being cut into 1–2 mm width strips. The strips were then minced and incubated on a shaker in 2.5 mg ml⁻¹ solution of collagenase (Sigma, C2674) in PBS at 37 °C for 2–3 h. The resulting solution was diluted 1 : 3 in PBS before centrifugation at 250 × g for 10 min. Floating adipocytes were removed and the remaining PBS aspirated from the cell pellet followed by resuspension and washing 2x in PBS. Red blood cells were removed by the addition of red blood cell lysis buffer (Sigma, R7757) for 2–3 min. Cells were then diluted with 30 ml PBS and centrifuged at 120 × g for 5 min, followed by aspiration of the supernatant and resuspension in 48 ml Dulbecco's modified eagle's medium (DMEM) with 10% fetal bovine serum. The resulting suspension was filtered twice through sterile gauze before additional centrifugation at 120 × g for 5 min and resuspension in 20 ml DMEM with 10% FBS. The cells were then filtered through a 100 μm nylon cell strainer (Fisher, 22363549), prior to counting with a hemacytometer (Reichert). Cells were then plated at 5–10 × 10³ cells per cm² in low glucose (1.0 g L⁻¹) DMEM with 10% fetal bovine serum prior to incubation in a low (5%) O₂ incubator. Cells were cultured for 48 h prior to the first media change, and passaged at confluency. Cell aliquots were frozen at less than passage 5.

Porcine adipose-derived stem cell culture and differentiation

Thawed ADSCs were cultured in low-glucose (1.0 g L⁻¹) DMEM with 10% FBS, penicillin-streptomycin, 2.9 g L⁻¹ L-glutamine, and 0.2 g L⁻¹ HEPES. Cells were cultured in an incubator maintained at 5% CO₂, 37 °C. ADSCs were passaged no more than 5 times. For PCEM imaging, ADSCs were washed with PBS (without Ca²⁺, Mg²⁺), trypsinized using 0.25% trypsin (Cell-Gro), and plated on PC biosensors in 2.0 ml at a density of 5.0 × 10⁴ cells/ml. To induce ADSC differentiation and development of dendrite-like cell projections, treated cells were exposed to a neurogenic induction medium containing 200 nM butylated hydroxyanisole (BHA), 2 mM valproic acid, 10 mM forskolin, 5 mg ml⁻¹ insulin, 2.5 mM KCl, and 25 mM hydrocortisone in solution with high-glucose (4.5 g L⁻¹) DMEM.¹⁶

Statistical analysis

Two-tailed student's *t* tests were performed for the results described in Fig. 2–3 with *p* < 0.05 used to signify statistical significance. All *p* value determinations were two-tailed. GraphPad software (LaJolla, CA) was used for all calculations concerning statistical evaluation. Error bars indicate one standard deviation from the mean.

Results

Dynamic label-free imaging of cell attachment

The imaging procedure is described in Fig. 1 using HepG2/C3 hepatic carcinoma cells. Selected images are cropped and

enlarged to show detail; cells were cultured on large (~1.75 cm²) sensor areas, and several 400 μm × 400 μm images were taken for each timepoint (see Supplementary Fig. 3 online). To demonstrate the ability of this label-free assay to detect cell attachment at a single-cell level, these images were cropped to the size of a few exemplary cells for the creation of each figure. The image shown in Fig. 1a was recorded at an angle below both cell and background resonance conditions, and provides morphological information similar to traditional bright field microscopy. Red and blue circles in Fig. 1a mark the locations of pixels for which transmission intensity is plotted as a function of angle of incidence in Fig. 1b. In Fig. 1c, the final PCEM image displays AMT for each pixel as a function of position presented as a false-color composite. Cell attachment shifts the local resonance to a lower value as indicated by the red color. The bright field image, used in tandem with the PCEM image, can be used to correlate structural and morphological information with the cell attachment spatial distribution (Fig. 1d).

Comparison of the brightfield image with the PCEM image shows an increased footprint area in the PCEM image attributed to a combination of the formation of lamellipodia and by the ability of the cell to alter the AMT of PC regions directly adjacent to it. In a previous study, similarly configured PC biosensors demonstrated a detection resolution of 3.5 μm in the direction parallel to the grating lines, and diffraction-limited resolution in the direction perpendicular to the grating lines¹¹ when an AMT shift 4x larger than those provided by typical cells was intentionally patterned on the PC surface with abrupt transition between high and low AMT. Based upon this earlier characterization, the cell attachment footprints measured by PCEM accurately reflect the cell boundaries within an uncertainty of ~2–3 μm in the direction parallel to the grating, and within ~1 μm in the direction perpendicular to the grating.

PCEM imaging is currently performed in a transmissive setup through the cell media, so it is likely that spatial resolution can be improved with the construction of a reflection-based detection instrument to avoid potential issues arising from sample-induced diffraction, scattering, and absorption. Scans completed in this study utilizes an incident angle scan range from 1.5°–2.0° at 0.01° increments. As each image takes approximately 50 ms to collect, it takes approximately 30 s to collect and save the images required to build a PCEM image for one frame. The computation required to compose the final image requires an additional ~15 s, allowing a final temporal resolution of approximately one frame per minute. As a result, cellular processes taking place on faster time scales may elude the PCEM processing modality in its current state, though scanning over a smaller range of angles or delaying image processing until conclusion of the study would result in moderate increases in sampling rate.

To demonstrate long-term application of PCEM, HepG2/C3 cells were plated on a poly-*d*-lysine (PDL)-coated sensor and the progress of their attachment was imaged *via* PCEM after 1, 2, 4 and 23 h in culture. After one hour in culture, the HepG2/C3 cells show evidence of cell attachment, presenting average AMT shifts of 0.25 ± 0.01° (1 S.D.) from background resonance. Throughout the time course, multiple changes in cell morphology can be seen in the bright field images, including changes in cell shape, size, and

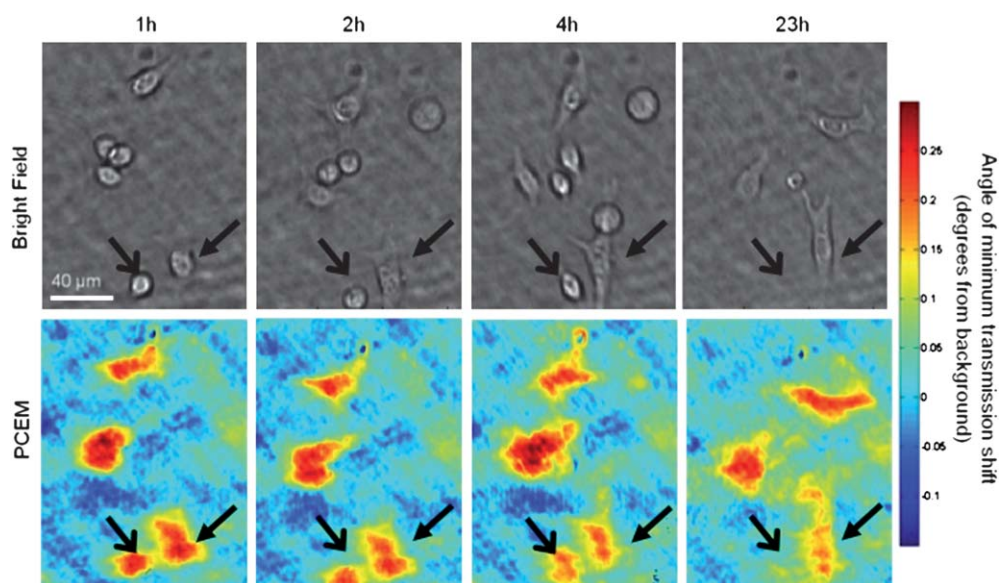


Fig. 2 PCEM observation of cell growth and movement. HepG2/C3 hepatic carcinoma cell growth and locomotion were recorded over a 23-hour period *via* PCEM. The PCEM timecourse shows evidence of cell migration (closed arrow) as well as of cell detachment (open arrow).

orientation throughout the experiment (Fig. 2). The PCEM images follow the changes in cell morphology observed in the bright field images, tracking the movement of the cell across the top of the field. Importantly, cells that translocate and cells that detach completely leave little to no evidence in the way of a footprint (Fig. 2, open arrows); this serves as further confirmation that the increased mass density causing AMT shift is caused by the presence of proteinaceous cell attachments, and not merely material adsorption from culture media or cellular secretion. Similarly, as cells spread and create more pronounced

attachments, areas of new attachment as indicated *via* brightfield microscopy show increased AMT shift *via* PCEM (closed arrows, Fig. 2). The relationship between PCEM images and bright field images lends PCEM extensive utility in tracking the relationship between dynamic cell activity and attachment footprint. At the 23-hour time point, PCEM images reveal that the cell areas interacting with the substrate are substantially larger than what may be inferred from bright field examination alone. Furthermore, the lateral resolution is sufficient to analyze variability of attachment within a single cell. The dark red color in the cell

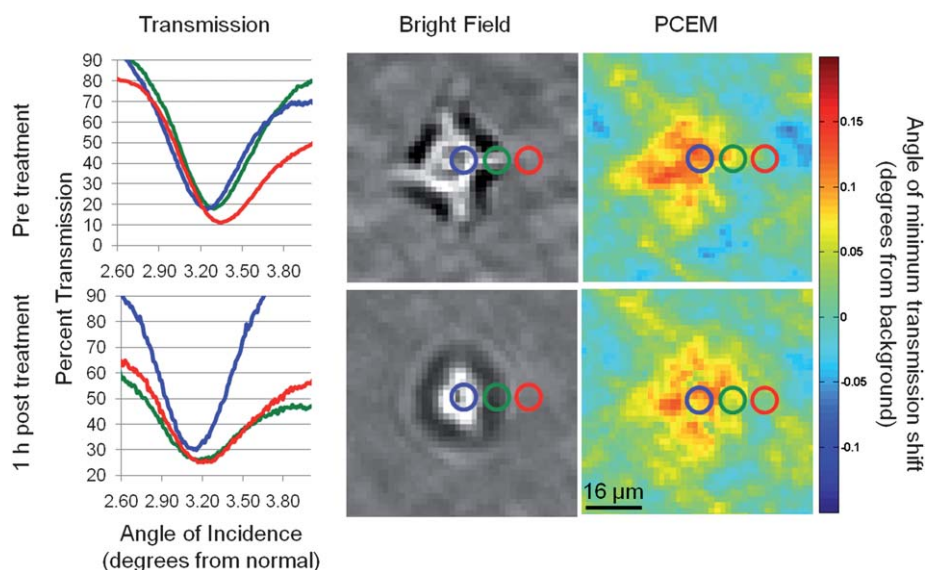


Fig. 3 PCEM can be used to detect changes caused by apoptosis. Three individual pixels were chosen from regions on the cell body (blue), on the cell periphery (green), and outside the cell boundary (red). Intensity of transmission at is plotted as a function of angle of incidence. Curves generated for pixels on the cell body and the cell periphery overlap before treatment with staurosporine, indicating the presence of protein-dense cell attachments in these regions. PCEM shows decreased cell attachment after induction of apoptosis *via* staurosporine administration, and retraction of peripheral cell attachments (green) is supported by PCEM data.

centers seen in the PCEM images indicates that attachment density is greatest at these locations.

Correlation with ECM-dependent physiologic changes

To demonstrate the ability of PCEM to resolve cellular changes in response to external stimuli, apoptosis was induced in Panc-1 human pancreatic cancer cells. Panc-1 cells were cultured on the sensor surface coated with PDL for 24 h before treatment with 10 $\mu\text{g/ml}$ staurosporine (Fig. 3). The morphological changes caused by staurosporine treatment are evident in the reduced definition of the cell border and rounded morphology shown in the bright field images. To characterize the cell response using PCEM, individual pixels were chosen from regions on the cell body (blue), on the cell periphery (green), and on the background (red). The selected regions are marked with circles on a bright field image and the curves for each pixel are given in the corresponding color in Fig. 3a. Prior to treatment, the curves for both pixels on the cell body and the cell periphery overlap and display an AMT shift of 0.10° from background. After treatment, the pixel residing on the cell periphery presents a curve more closely resembling that of the background, indicating decreased protein density at this location. The cell body remains on the surface, but causes a smaller AMT shift from background, indicating a weakening of attachment. Finally, PCEM images display the decrease in attachment across the cell, as indicated by a lower AMT shift from background. This provides confirmation that cell attachment does not permanently alter the sensor surface but rather presents a transient increase in dielectric permittivity for the duration of cell attachment at that location on the biosensor.

Another interesting application of PCEM is concurrent monitoring of cell physiology, morphology, and attachment density. Cardiomyocytes require fibronectin-dependent integrin-mediated cell attachments for optimal development and contractility.¹² To verify that PCEM is capable of detecting significant differences in cell attachment caused by changes in the available ECM substrate, primary neonatal rat cardiomyocytes were isolated and cultured on an uncoated PC biosensor and on a biosensor coated with a combination of collagen and fibronectin.¹³ At 24 h the cells were imaged *via* PCEM, and their morphologies and beating rates were recorded (see Supplementary Fig. 6 online†). Cells cultured in the absence of fibronectin showed greater frequency of rounded morphology, and showed a complete lack of contractility (Fig. 4a, 4b). Cells cultured in the context of both fibronectin and collagen, however, showed a significantly greater frequency of stretched morphology, and exhibited an increased proportion of contractile cells (Fig. 4b). Additionally, contractility was exhibited only among cells showing a stretched morphology, supporting the fact that fibronectin-dependent cell attachment is critical for cardiac myocyte growth and differentiation. AMT shift was evaluated over 70- to 100- pixel regions on and off each cell, enabling local background comparisons to be performed for each cell (see Supplementary Table 1 online†). PCEM results confirmed the morphological observations, as cardiomyocytes exhibiting stretched morphology showed the greatest amount of AMT shift from background, and significantly greater amounts of AMT shift in comparison to their rounded counterparts, independent

of the coating applied to the sensor surface (Fig. 4b, $p = 0.0133$ and $p < 0.0001$ for coated and uncoated sensors, respectively).

Characterization of stem cell differentiation

To demonstrate the capacity of PCEM for label-free assessment of cell differentiation, we exposed porcine adipose-derived stem cells to a neurogenic induction medium, performing PCEM before and after administration. The induced morphological changes are typical of neurogenic differentiation, characterized by retraction of the cell body and the development of small, dendrite-like cellular projections^{14,15} (Fig. 4c). These changes were accompanied by a significant reduction in cell attachment as determined by a decrease in AMT shift (Fig. 4d, $p = 0.0007$). As the neurogenic induction protocol stimulates remodeling of the cytoskeleton and cell attachments, decreased attachment protein density is to be expected. The agreement of PCEM with this assertion demonstrates that the technique can be used to characterize the progression of stem cell differentiation without disturbing the process with fluorescent labels or cytotoxic endpoint assays.

This work demonstrates several new capabilities of PC biosensors using PCEM. The technique is capable of visualizing dynamic cell attachment with a pixel resolution of less than one micron, enabling highly detailed quantification of attachment distribution within individual cells. The label-free aspect of PCEM enables the prolonged study of cell-ECM attachment evolution in the context of cell growth, locomotion, differentiation, and apoptosis. The ability to functionalize PC biosensors with multiple cell-amenable coatings allows the study of the effects of substrate composition on cell attachment. PCEM also allows direct comparison between bright field and PCEM images, enabling correlation of cellular morphology with changes in attachment density. This combination of capabilities provides a unique new tool for study of cell attachment in many contexts, including wound healing, cell culture optimization, stem cell differentiation, and cancer metastasis.

Discussion

The importance and utility of label-free imaging have recently been underscored by an expansion in the number of techniques to acquire such data as well as by a growing need for improved understanding for a number of cellular processes. The use of fluorescent and chemical labels remains invaluable for the study of specific proteins and biochemical interactions, but the specificity such techniques provide often comes at the cost of decreased cell viability and a limited ability to study the same cells over extended periods of time. Such techniques also necessitate the use of one or several exogenous chemical markers in the area of interest within the cell, which introduces the possibility of obscuring the phenomenon of interest as it occurs in the absence of such labels. With the emergence of label-free techniques including surface plasmon resonance imaging (SPRi) and ellipsometric microscopy, it has become possible to gain information complementary to that provided by traditional light microscopy. By decreasing the complexity of the experimental system, these techniques are in fact capable of investigating model systems with greater fidelity to their *in vivo* counterparts.

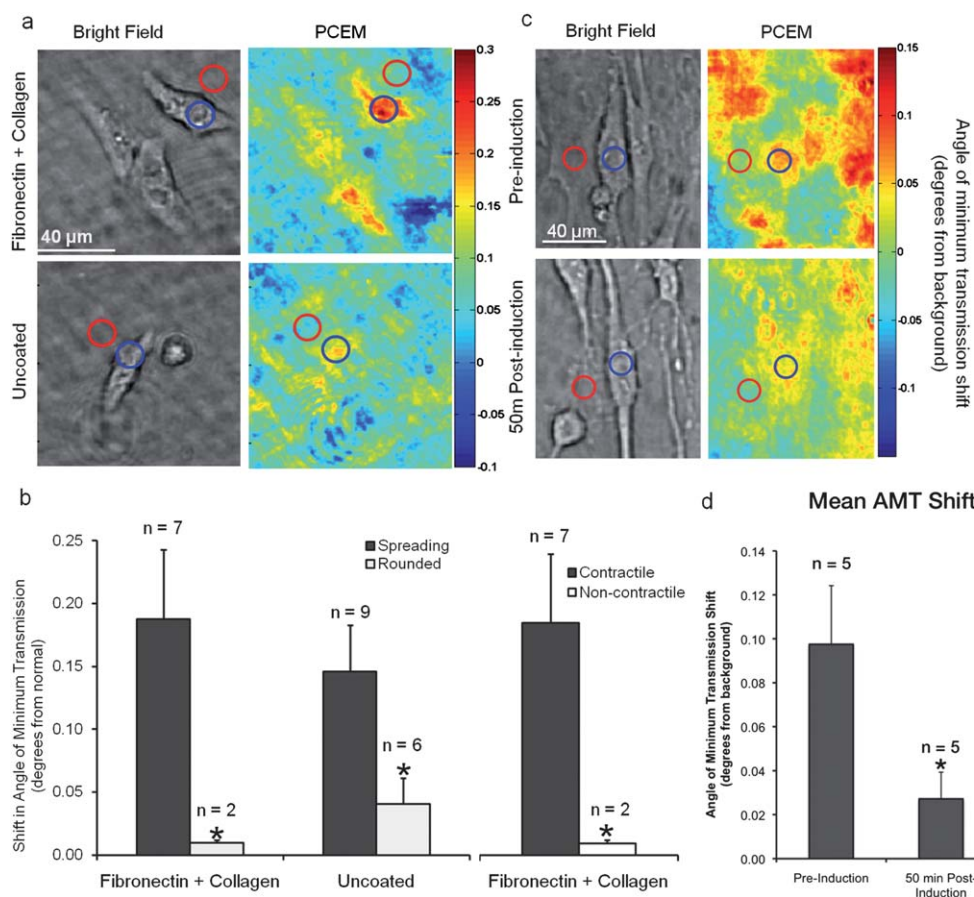


Fig. 4 PCEM imaging of cellular responses brought about by extracellular stimuli. Blue circles indicate sample regions of interest used to measure AMT on individual cells, while red circles indicate sample regions of interest used to perform local background AMT measurements. a) Cropped bright field and corresponding PCEM images are shown for neonatal rat cardiomyocytes in culture on uncoated as well as fibronectin- and collagen-coated PC biosensors. b) On both coated (fibronectin + collagen) and uncoated sensors, cells exhibiting stretched morphology showed greater AMT shift than their rounded counterparts ($p = 0.0133$ and $p < 0.0001$, respectively). Contractile cells also exhibited significantly greater AMT shift than non-contractile cells cultured on coated sensors ($p = 0.0133$). c) Forced differentiation of porcine adipose-derived stem cells with neurogenic induction medium stimulates the production of dendrite-like cell projections and retraction of cell bodies. d) Cells prior to treatment showed significantly greater attachment protein density than cells after treatment ($p = 0.0007$).

Despite this advantage, label-free imaging technologies continue to work against several challenges. While SPRi has enjoyed the ease of implementation associated with traditional surface plasmon resonance scanning techniques, one persistent area of difficulty is brought about by the lateral propagation of surface plasmons, which occurs on the order of several tens of microns.¹⁷ This restricts the spatial resolution achievable with SPRi to distances on the order of entire cells, limiting the possibilities for its use in subcellular imaging. Similarly, ellipsometric imaging techniques have met with moderate success due to the comparatively small refractive index differences present in biological samples surrounded by aqueous media. PC biosensors seem to make several of these problems more tractable – it is possible to construct PC-based sensors with propagation lengths of less than 5 microns, and sensors generally exhibit high sensitivity with regard to biological samples including proteins, nucleic acids, and whole cells immersed in aqueous media.⁴

As the PCEM instrumentation registers shifts in transmitted wavelengths rather than changes in intensity, PCEM remains insensitive to the detection of particles passing transiently

through the field of view. This represents another advantage over intensity-based detection assays, which may demonstrate susceptibility to artifacts in the presence of soluble particles capable of absorbing wavelengths of interest for analysis. Materials that adsorb to the sensor surface that also strongly absorb light at the laser wavelength have been documented to extinguish the PC resonance. In such a case, the resonance disappears, and the AMT fitting algorithm no longer functions.¹⁸ Such regions can be automatically recognized by the instrument software. Although no such cases were observed for the experiments conducted in this work, this technique has been used to measure deposition of light-absorbing hydroxyapatite produced by surface-attached stem cells that have differentiated to become osteoblasts.

In this work, we demonstrated PCEM as a useful tool to study a number of biologically interesting questions regarding cell attachment in several contexts. Because this new technique grants access to previously unavailable information, it will allow the achievement of a greater level of understanding not only in fundamentally interesting areas of cell biology, but also clinically

relevant questions such as what types of cellular changes enable cancer metastasis, and what kinds of biomaterials and biocompatible polymers might best be applied to increase wound healing and recovery in the absence of inflammation and scarring. Questions such as these will require an unprecedented understanding of the extracellular matrix as well as of the cells interacting with that ECM. In future work, PCEM may be used in combination with existing technology to increase our understanding of the biology underlying problems like cancer metastasis, wound healing, axonal repair, and ischemic damage. The combination of PCEM with specific fluorescence labeling, for example, will allow the investigation of individual protein and signaling interactions in such contexts with respect to their influence on cell attachment. Modeling disease systems and using recently developed biomaterials on PC biosensors with this new technique will allow new insight into these problems, enabling researchers to develop more successful therapeutic approaches to clinical disease.

Acknowledgements

We are grateful for support provided by the U.S. Army Medical Research & Materiel Command (USAMRMC), the Telemedicine & Advanced Technology Research Center (TATRC) under Contract No. W81XWH0810701. Resources and support supported by the University of Illinois Center for Nanoscale Science and Technology and the US. Army Engineering Research and Development Center, Construction Engineering Research Laboratory (ERDC-CERL) are thankfully acknowledged. Additionally, we are thankful for the support of the National Science Foundation (NSF) Integrative Graduate

Education and Research Traineeship (IGERT) in Cellular and Molecular Mechanics and BioNanotechnology (CMMB IGERT 0965918).

References

- 1 N. J. Boudreau and P. L. Jones, *Biochem. J.*, 1999, **339**, 481–488.
- 2 M. Barczyk, S. Carracedo and D. Gullberg, *Cell Tissue Res.*, 2010 Jan, **339**(1), 269–80.
- 3 B. T. Cunningham, P. Li, B. Lin and J. Pepper, *Sens. Actuators, B*, 2002, **81**(2–3), 316–328.
- 4 B. T. Cunningham, *et al.*, *J. Biomol. Screening*, 2004, **9**(6), 481–490.
- 5 P. Y. Li, B. Lin, J. Gerstenmaier and B. T. Cunningham, *Sens. Actuators, B*, 2004, **99**, 6–13.
- 6 L. Chan, S. Gosangari, K. Watkin and B. T. Cunningham, *Apoptosis*, 2007, **12**(6), 1061–1068.
- 7 A. W. Petersen, M. Halter, A. Tona, K. Bhadriraju and A. L. Plant, *BMC Cell Biol.*, 2009, **10**, 16.
- 8 Y. Yanase, *et al.*, *Biosens. Bioelectron.*, 2010, **26**(2010), 674–681.
- 9 M. Bivolarska, T. Velinov and S. Stoitsova, *J. Microsc.*, 2006, **224**(3), 242–248.
- 10 D. Marinkovaa, *et al.*, *Colloids Surf., B*, 2008, **65**, 276–280.
- 11 I. D. Block, P. C. Mathias, S. I. Jones, L. O. Vodkin and B. T. Cunningham, *Appl. Opt.*, 2009, **48**(34), 6567–6574.
- 12 I. D. Block, P. C. Mathias, N. Ganesh, S. I. Jones, B. R. Dorvel, V. C. Chaudhery, L. O. Vodkin, R. Bashir and B. T. Cunningham, *Opt. Express*, 2009, **17**(15), 13222–13235.
- 13 A. Mikson, T. Ehashi, A. Mahara, H. Uyama and T. Yamaoka, *J. Artif. Organs*, 2009, **12**(2), 111–117.
- 14 A. H. Maass and M. Buvoli, *Methods Mol. Biol.*, 2007, **366**, 321–30.
- 15 K. M. Safford, *et al.*, *Biochem. Biophys. Res. Commun.*, 2002, **294**, 371–379.
- 16 T. Huang, D. He, G. Kleiner and J. Kuluz, *J. Spinal Cord Med.*, 2007, **30**(S1), S35–40.
- 17 M. E. Caldwell and E. M. Yeatman, *Appl. Opt.*, 1992, **31**(20), 3880–289.
- 18 S. Shamah and B. T. Cunningham, *Analyst*, 2011, **136**, 1090–1102.